Lunar and Mars orbital stereo image mapping

Man Peng, Zongyu Yue, Yiliang Liu, Kaichang Di*
State Key Laboratory of Remote Science, Institute of Remote Sensing Applications, Chinese Academy of Sciences, Beijing 100101, China

ABSTRACT

Orbital image mapping is a key technology to achieve scientific and engineering goals in deep space exploration missions. It provides topographic and morphological information for various scientific researches and also supports follow-up landing missions. This paper presents rigorous photogrammetric models for Chang'E-1 and MRO HiRISE images based on the pushbroom imaging principle. A multi-level stereo image matching method is developed in order to generate high precision DEMs of lunar and Mars surfaces.

Keywords: Chang'E-1 orbiter, HiRISE, Pushbroom, Stereo mapping

1. INTRODUCTION

Orbital image mapping is an important basic task in deep space exploration such as lunar and Mars exploration. It supports various scientific researches and provides topographic information for landing-site selection, precision landing and surface operation in following-up landing missions. China's first lunar probe Chang'E-1 (CE-1) was successfully launched on October 24, 2007 and operated until March 1, 2009. The three line CCD stereo camera onboard CE-1 acquired images of the entire lunar surface, which provided fundamental information for lunar research and the consequent lunar exploration in China [1][2].

So far the most noticeable orbiter for mars exploration is NASA's Mars Reconnaissance Orbiter (MRO), which entered Mars orbit on March 10, 2006. With an unprecedented high resolution of 0.25 m, the HiRISE (High Resolution Imaging Science Experiment) camera onboard MRO provides detailed topographic, morphological and spectral information for Mars research and landing-site selection for the next Mars rover [3].

The research and development of planetary orbiter mapping started in 60's of last century along with the launches of lunar and Mars exploration probes by the U. S and former USSR [4]. In recent years many research have been conducted on the geometric modeling and stereo mapping from pushbroom sensors. Eliason et al. created a global lunar mosaic using Clementine 750mm channel images [5]. Rosiek et al. completed color-coded topographic and shaded relief mesh maps of the Moon with a scale of 1:10,000,000 [6]. Most recently, Kirk *et al.* developed a rigorous geometric model for HiRISE imagery and generated 3D maps at Phoenix landing site [7]. Li *et al*. developed a rigorous photogrammetric model and performed a bundle of adjustments and topographic mapping at Spirit rover's landing site [8]. The Mapping and GIS laboratory at the Ohio State University produced a DEM of Apollo 16 landing site using images of Lunar Reconnaissance Orbiter Camera (LROC) with a 0.5m resolution [9].

Moreover, researchers in China have also studied lunar orbiter imaging geometry and 3D mapping methods. Wang et al. applied three-line array photogrammetry principle to lunar mapping and performed a simulation experiment using Apollo orbiter data [10]. Zhao et al. developed a pyramid based matching method for three-line array images and demonstrated its feasibility and efficiency using simulated data[11]. Cui et al. proposed a method for topographic modeling through space resection and intersection without control points and satellite orientation information[12]. Li et al. summarized CE-1 image acquisition and data quality and described the data processing procedure for generation of China's global lunar image map with a scale of 1:2,500,000[2].

This paper presents rigorous photogrammetric models for Chang'E-1 and MRO HiRISE images based on the pushbroom imaging principle. A multilevel image matching method is developed for dense matching of stereo images. Consequently DEMs of lunar and Mars surfaces are automatically generated.

* Corresponding Author: Kaichang Di; kcdi@irsa.ac.cn; phone/ fax 86 10-64868229

Remote Sensing of the Environment: The 17th China Conference on Remote Sensing, edited by Qingxi Tong, Xingfa Gu, Boqin Zhu, Proc. of SPIE Vol. 8203, 820304

2. GEOMETRIC MODELING OF PUSHBROOM IMAGING SENSORS

2.1 Interior orientation

In order to perform topographic mapping from orbital stereo images, firstly calibrated interior-orientation parameters are used to calculate focal plane coordinates from pixel coordinates.

2.1.1 Imaging geometry of CE-1 stereo imagery

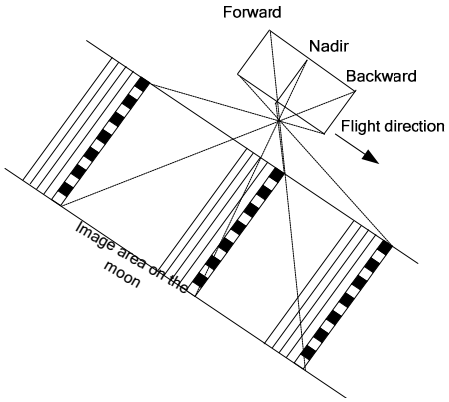

Fig. 1. CE-1 stereo camera imaging configuration [2]

The CE-1 CCD camera is a three line pushbroom camera which is implemented on an area array CCD sensor. The CCD array has 1024×1024 pixels, with each pixel being $14\mu m * 14\mu m$ in the chip. The forward-, nadir- and backward-looking images of the Moon surface are generated by reading the 11th, 512th and 1013th rows that are perpendicular to the flight direction (Fig.1). The convergence angle between the adjacent views is 16.7°. At a 200 km altitude, the image spatial resolution is 120 m and the swath width is about 60 km. The focal length of the CCD camera is 23.33 mm.

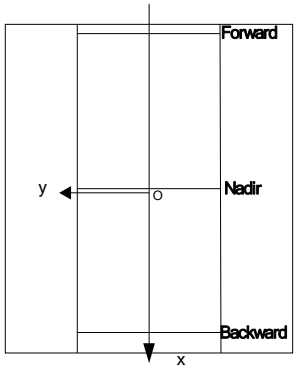

Fig. 2. Focal plane frame of the CE-1 CCD

The actual imaging area is 1024 rows by 512 columns. The focal plane frame is shown in Fig.2. The pixel coordinates are transformed to the focal plane frame with the following equations:

$$\begin{aligned} x_{backward} &= (x_p - 11) * pixelsize - x_0 \\ x_{nadir} &= (x_p - 512) * pixelsize - x_0 \\ x_{forward} &= (x_p - 1013) * pixelsize - x_0 \\ y_{backward} &= y_{nadir} = y_{forward} = (y_p - col) * pixelsize - y_0 \end{aligned} \tag{1}$$

where ($x_{forward}$, $y_{forward}$) represent focal plane coordinates in the forward-looking image; (x_{nadir}, y_{nadir}) are focal plane coordinates in the nadir-looking image; ($x_{backward}$, $y_{backward}$) are focal plane coordinates in the backward-looking image; (x_p, y_p) are the center position (511.5, 255.5) of the actual imaging area; (x_0, y_0) represent the principal point position in the focal plane frame; pixelsize is 0.014 mm/pixel; *col* is the pixel position in the column direction.

2.1.2 HiRISE imaging geometry

Being different from CE-1, HiRISE is a pushbroom imaging sensor with 14 CCDs (10 red, 2 blue-green and 2 NIR). As shown in Fig.3, ten CCDs covering the red spectrum are located in the middle of the focal plane, with overlaps of 48 pixels between adjacent CCDs. The resolution of HiRISE images is 25cm/pixel at the altitude of 300 km[3]. At such a high resolution, the IFOV (instantaneous field-of-view) is extremely small. To improve the signal strength of "fast-moving" objects and to increase the exposure time, Time Delay Integration (TDI) technology was incorporated in the instrument.

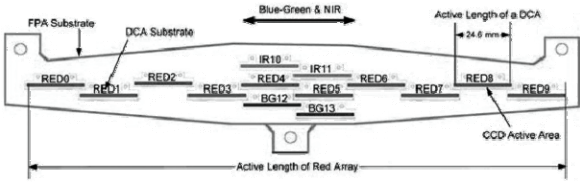

Fig. 3. Layout of HiRISE CCDs [7]

According to the HiRISE instrument kernel which provides the calibrated interior orientation parameters[7], the position of each pixel can be transformed to focal plane coordinate with the following equations:

$$\begin{aligned} x &= x_{i0} + x_{i1} * (\text{ccdsample\_c+off\_s-cen\_s}) + x_{i2} * \text{ccdLine\_c} \\ y &= y_{i0} + y_{i1} * (\text{ccdsample\_c+off\_s-cen\_s}) + y_{i2} * \text{ccdLine\_c} \end{aligned} \tag{2}$$

where (x, y) are image coordinates in the focal plane with respect to HiRISE optical center; x_{i0}, x_{i1}, x_{i2} y_{i0}, y_{i1}, y_{i2} are calibrated parameters; off_s=0 is for channel 1 and off_s=1025.0 is for channel 0; cen_s is the column center of CCD; $ccdSample\_c$ is the un-binned pixel index from binned pixels with respect to the image center; $ccdLine\_c$ is the un-binned number of the CCD line in the middle of TDI block.

Radial lens distortion is calculated as

$$\begin{aligned} r &= \sqrt{x^2 + y^2} \\ \Delta x &= -x(k_0 + k_1 * r^2 + k_2 * r^4) \\ \Delta y &= -y(k_0 + k_1 * r^2 + k_2 * r^4) \end{aligned} \tag{3}$$

where $\Delta x, \Delta y$ are the corrections of the image coordinates; k_0, k_1, k_2 are lens distortion parameters.

Finally, the calibrated image coordinates ($x^{'}, y^{'}$) are calculated as

$$\begin{aligned} x^{'} &= x + \Delta x \\ y^{'} &= y + \Delta y \end{aligned} \tag{4}$$

2.2 Exterior orientation

After interior orientation, exterior orientation is needed to establish the relationship between the focal plane frame and lunar/Mars body-fixed frame (LBF/MBF). As the frequency of telemetry exterior orientations parameters (EOPs) from satellite tracking is much lower than that of CCD scanning, the EOPs of each image line should be obtained by interpolation using the spacecraft's trajectory and pointing vectors. The exterior orientation procedure is shown in Fig.4.

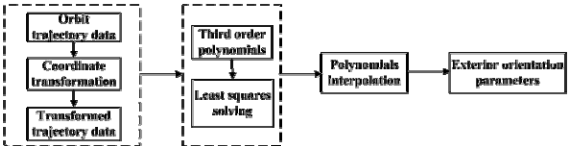

Fig. 4. Procedure of exterior orientation

Since the orbit trajectory data are defined in J2000 frame and topographic mapping product is usually referenced to LBF/MBF, the EOPs need to be firstly transformed from J2000 to LBF/MBF using Eq. (5)：

$$\begin{aligned} R_{IAU}^{INS} &= R_{IAU}^{J2000} R_{J2000}^{INS} \\ A_{IAU} &= R_{IAU}^{J2000} A_{J2000} \end{aligned} \tag{5}$$

where R_{IAU}^{INS} is the rotation matrix between focal plane frame and LBF/MBF; R_{J2000}^{INS} is the rotation matrix between the focal plane frame and J2000; R_{IAU}^{J2000} is the rotation matrix between J2000 and LBF/MBF; A_{J2000} is the position of the CCD perspective center in J2000; A_{IAU} is the position of the CCD perspective center in LBF /MBF.

Secondly, we need to model the EOPs so that EOPs of each scan line can be computed by interpolation. Previous research has shown that changes of EOPs over a short trajectory of a pushbroom sensor can be well modeled using polynomials[13]. Experimental results also show that second order polynomial achieves lower accuracy. So we use third order polynomial to model the EOPs w.r.t. time t.

$$\begin{aligned} X(t) &= a_0 + a_1 t + a_2 t^2 + a_3 t^3 \\ Y(t) &= b_0 + b_1 t + b_2 t^2 + b_3 t^3 \\ Z(t) &= c_0 + c_1 t + c_2 t^2 + c_3 t^3 \\ \omega(t) &= d_0 + d_1 t + d_2 t^2 + d_3 t^3 \\ \varphi(t) &= e_0 + e_1 t + e_2 t^2 + e_3 t^3 \\ \kappa(t) &= f_0 + f_1 t + f_2 t^2 + f_3 t^3 \end{aligned} \tag{6}$$

where X(t), Y(t), Z(t) are the positions of the perspective center in LBF/MBF at time t; $\omega(t), \varphi(t), \kappa(t)$ are pointing angles of the focal plane in LBF/MBF at time t; $a_0, \ldots, f_3$ are polynomial coefficients; t is the acquisition time of each line.

According to trajectory data, least squares principle is used to solve polynomial coefficients. Consequently, the position and attitude of each line can be calculated using Eq. (6) with the imaging time of each line and polynomial coefficients.

To check the applicability and accuracy of third order polynomials, we examined the trajectory and pointing data of 562nd orbit of CE-1 (acquired between 00:23:32.001 and 00:26:22.00 on Oct 26, 2007). For comparison purposes, we used both second and third order polynomials. The residuals of the trajectory and pointing data are shown in Fig.5, where it can be seen that third order polynomial model fits the position parameters well. The root mean square errors (RMSEs) are listed in Table 1.

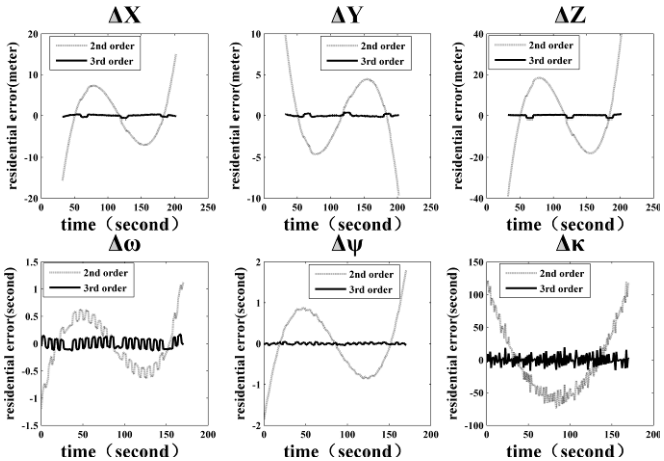

Fig. 5. Residuals of polynomial fitting for orbit trajectory and pointing data

Table 1. RMSE of polynomial fitting of EOPs

Polynomial order	Position (meter)			Orientation (second)		
	X	Y	Z	Ω	φ	K
2	6.03	3.82	15.4	0.45	0.72	53.59
3	0.23	0.14	0.57	0.09	0.02	7.62

From the figures and the tables, it can be easily observed that third order polynomials are much better than second order polynomials in modeling the EOPs. Smaller residuals reveal that the position and attitude of the satellite platform change stably.

3. STEREO IMAGE MATCHING

To generate topographic product after rigorous modeling, the image matching is needed to provide homologous points from stereo images. Then, 3D points can be calculated by the space intersection with the EOPs and DEM can be interpolated from these 3D points. We developed a multi-level image matching method. The flowchart is shown in Fig.6.

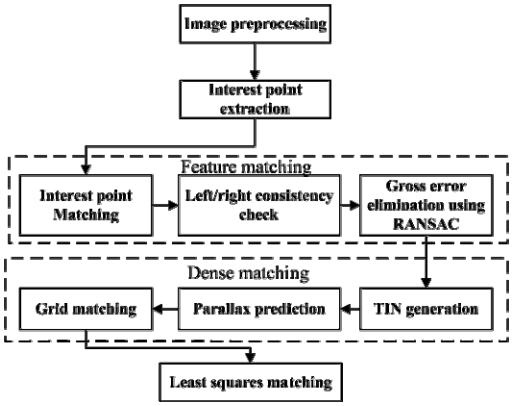

Fig. 6. Multi-level stereo image matching

Radiometric enhancement is conducted using Gaussian filter and histogram normalization to remove noises and illumination difference. Interest points are generated by Förstner operator according to Eq. (7) and matched using normalized correlation coefficients.

$$F(g) = \frac{g_x^2 g_y^2 - g_{xy}^2}{g_x^2 + g_y^2} \tag{7}$$

where F(g) is the interest vale of an image point; g_x, g_y are 1D gradients of point(s); g_{xy} is 2D gradient.

Matching error detection is performed using left/right consistency check. As shown in Fig.7, from the left image to the right image, P1 matches Q1, and P2 matches Q2; from the right image to the left image, Q1 matches P1, and Q2 matches P3. Through the left/right consistency check, (P1, Q1) are accepted as correct matches, while (P2, Q2) and (Q2, P3) are discarded as mismatches.

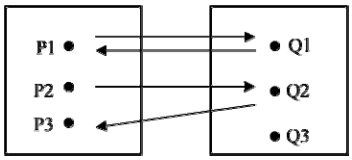

Fig. 7. Left/right consistency check

To ensure the reliability of interest point matching, a RANSAC process[14] is applied to eliminate gross errors further using a 2D similarity transformation model in a local area:

$$\begin{bmatrix} x_r \\ y_r \end{bmatrix} = \begin{bmatrix} a & -b \\ b & a \end{bmatrix} \begin{bmatrix} x_l \\ y_l \end{bmatrix} + \begin{bmatrix} c \\ d \end{bmatrix} \tag{8}$$

where x_l, y_l are image coordinates of the left (forward-looking) image; x_r, y_r are image coordinates of the right (backward-looking) image; a, b, c, d are transformation coefficients.

After matching of interest points, a triangulated irregular network (TIN)-controlled dense image matching method is adopted for dense grid matching. Firstly, a TIN is generated from the matched interest points on the left image, and the x- and y- parallaxes are calculated at each vertex. Second, a grid of 3×3 pixels is generated in the left image and the homologous image point of each grid point on the right image is predicted using linear interpolation of parallaxes from vertices of the triangle that covers the grid point. The actual homologous point in the right image is determined by cross correlation within a small search range from the predicted position. At last, least squares matching method is applied to reach sub-pixel accuracy. After image matching, 3D positions of the matched points are calculated using space intersection with the co-llinearity equations. The final DEM was generated using Kriging interpolation.

4. EXPERIMENT RESULTS

4.1 Lunar mapping using CE-1 images

The developed method is tested using CE-1 stereo images of a 61 km × 120 km area. The image is 512 Columns by 1001 rows and centered at 30°N and 46°W. The forward- and backward-looking images are shown in Fig. 8(a) and 8(b) respectively.

After the interest point matching, 564 points are matched, and after the dense matching using a grid of 3×3 pixels 47,835 points are matched. Part of the TIN and dense points are shown in Fig. 8(c) and Fig. 8(d). In order to show the terrain map more directly, 3D coordinates in LBF are transformed into longitude, latitude and altitude. Fig. 9 is a perspective view of the generated DEM with a 500 m resolution. Unlike the situation on Earth, no absolute ground truth is available on the lunar surface. Therefore, the accuracy of DEM can't be checked with ground truth. Instead, back-projection residuals in the image space are used to evaluate the accuracy of the DEM. The RMSE of differences between the measured image points and the corresponding back-projected image points is 0.146 pixel, which represents a sub-pixel accuracy of the mapping product.

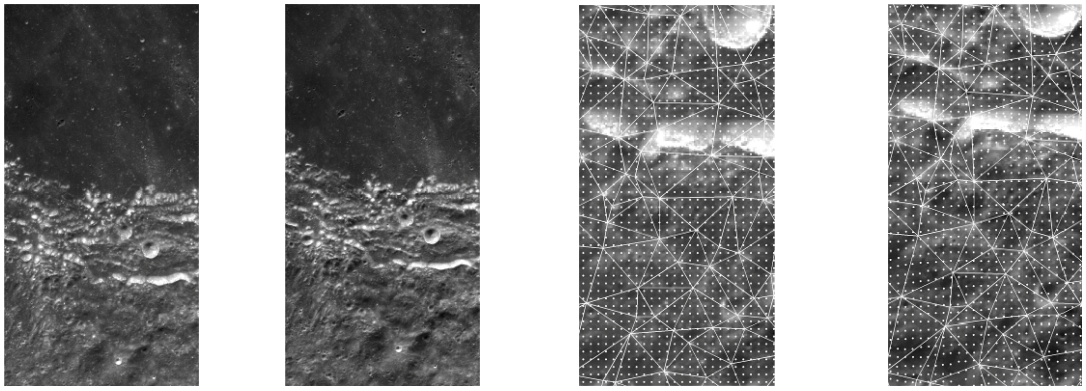

(a) (b) (c) (d)

Fig. 8. (a) The forward image; (b) the backward image;(c) dense points in the forward image;(d) matched dense points in the backward image

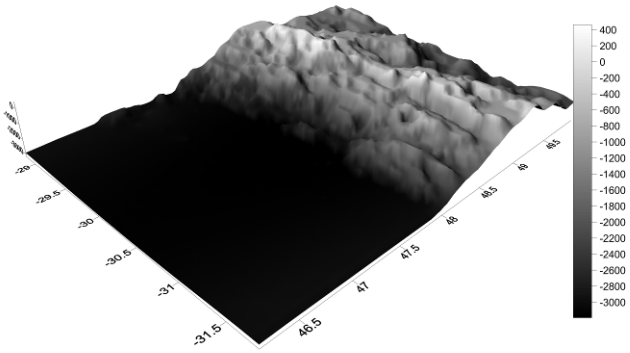

Fig. 9. Perspective view of the generated CE-1 DEM

4.2 Mars mapping using HiRISE images

HiRISE EDR (Experiment Data Record) data can be downloaded from the official website of HiRISE (http://marsoweb.nas.nasa.gov/HiRISE/hirise_images/) or PDS (The Planetary Data System) website (http://pds-imaging.jpl.nasa.gov/). The images used in the experiment are shown in Fig. 10 (a) and Fig.10(b); the ID numbers are SP_001777_1650_RED0_0 (1650) and PSP_001513_1655_RED0_0 (1655), respectively. The data acquisition dates are December 12, 2006 and November 12, 2006. The orientation parameters are extracted from IK, SPK and CK files from NAIF (Navigation and Ancillary Information Facility)). Fig. 10(c) shows the automatically generated DEM with a 1 m resolution. By comparing the back-projected image and matched points, the RMSE is 0.009 pixel, which shows a good accuracy.

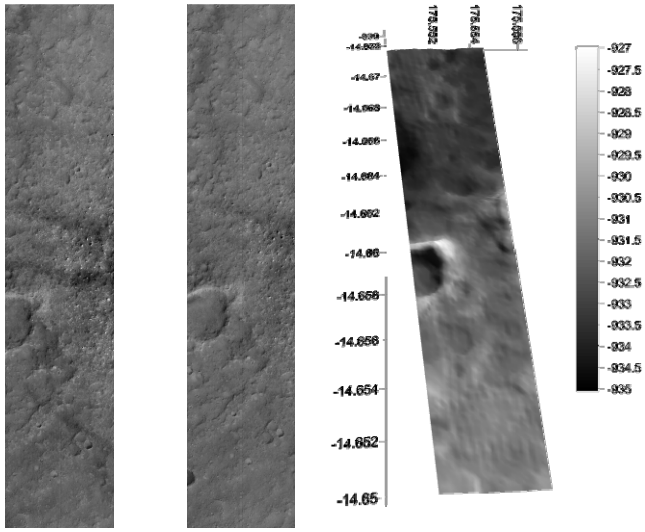

(a) (b) (c)

Fig. 10. (a) HiRISE image 1650; (b) HiRISE image 1655; (c) generated HiRISE DEM

5. CONCLUSIONS

In this paper, we present a rigorous photogrammetric processing approach of automatic DEM generation from pushbroom orbital imagery for lunar and Mars mapping. Rigorous photogrammetric models for CE-1 and HiRISE imagery are developed, and then a coarse-to-fine multilevel dense matching method is employed to provide dense points

for DEM generation. Consequently DEM is generated by Kriging interpolation. Experimental results using CE-1 and HiRISE stereo images are satisfactory.

ACKNOWLEDGEMENTS

Funding of this research by National High Technology Research and Development Program of China (Contract No. 2009AA12z310) and National Natural Science Foundation of China (Grant No. 40871202) is acknowledged.

REFERENCES

[1] Ouyang Z., Li C., Zou Y. et al., "The Primary Science Results from the Chang'e-1 Probe", Sci China Earth Sci, 40(3), 261-280 (2010).

[2] Li C., Liu J., Ren X. et al., "The global image of the Moon obtained by the Chang'E-1:Data processing and lunar cartography," Sci China Earth Sci, 40(3), 294-306 (2010).

[3] Mcewen A. S., Eliason E. M., Bergstrom J. M. et al., "Mars Reconnaissance Orbiter's High Resolution Imaging Science Experiment (HiRISE)," Journal of Geophysical Research Planets, 112 (2007).

[4] Greeley R. and Batson R. M., [Planetary Mapping], Cambridge Press, 100-105 (2007).

[5] Eliason E., Isbell C. and Lee E., "Mission to the Moon: The Clementine UVVIS global lunar mosaic", Houston Lunar and Planetary Institute(1999).

[6] Rosiek M. R., Kirk R. L. and Howington-Kraus, "Color-coded topography and shaded relief maps of the lunar hemispheres," 33rd Lunar and Planetary Science Conference, Houston: Lunar and Planetary Institute, (2002).

[7] Kirk R., L., Rosiek M. R., Anderson J. A. et al., "Ultrahigh resolution topographic mapping of Mars with MRO HiRISE stereo images: Meter-scale slopes of candidate Phoenix landing sites," Journal of Geophysical Research Planets, 113(24), (2008).

[8] Li R., Hwangbo J.W., Chen Y. and Di K., "Rigorous photogrammetric processing of HiRISE stereo images for mars topographic mapping," the International Archives of the Photogrammetry, Remote Sensing and Spatial Information Sciences, 37(B4), 987-992(2008).

[9] LROC team, http://lroc.sese.asu.edu/news/? archives/97-First-LROC-Stereo-Results.html

[10] Wang J., Wang X., Li J. et al., " Application of three-line array CCD photogrammetry theory to lunar exploration," 33(6), 19-20(2008)

[11] Zhao F., Hu S., Guan Z. and Zhu X., "Study of automatic matching technology of image points for three line array CCD imaging," Science of surveying and mapping, 33(4),12-14(2008)

[12] Cui T., Chen S. and Wang J., "Three dimensional modeling of the lunar surface based on stereo camera onboard Chang'E orbiter," Remote sensing for land resources, 82(4), 31-34(2009).

[13] Yoon, J. and Shan J., "Combined adjustment of MOC stereo imagery and MOLA altimetry data," Photogrammetric Engineering and Remote Sensing, 71(10), 1179–1186(2005).

[14] Fischler M.A. and Booth R. C., "Sample consensus: a paradigm for model fitting with applications to image and automated cartography," Graphics and Image Processing, 24(6), 381-395(1981).